CrossMark

Cu and/or Ni catalysts over CePr oxide for the water gas shift reaction: an experimental study, kinetic fitting and reactor simulation

Eduardo Poggio-Fraccari[1] (ORCID) · **Pablo Giunta**[1] ·
Graciela Baronetti[1] · **Fernando Mariño**[1]

Abstract Several Cu and Ni samples, supported over Pr-promoted ceria, were characterized and tested as water gas shift (WGS) catalysts in the temperature range 250–450 °C. Three metal loadings were studied, 5, 10 and 20 wt%. Redox (TPR) and textural (XRD and BET) properties were correlated with the observed catalytic behavior. The activity clearly increased with metal loading (Cu or Ni) from 5 to 10 wt%, but no major changes were observed between mid and high metal loading samples, 10 and 20 wt%. This might be due to appreciable metal segregation over support surface as Cu or Ni content increases. For Ni-containing samples, CH_4 was found at the reactor outlet stream, showing that CO methanation also takes place. For 10 wt% total metal content, kinetic expressions for monometallic Cu and Ni catalysts, and a bimetallic CuNi were proposed and fitted simultaneously for both WGS and the CO methanation reaction. Then, the kinetic expressions were used to model a reactor scheme where the main goal was the minimization of the required catalyst mass for a given CO conversion. It can be concluded that the most promissory scheme consists of two reactors, the first operating with the CuNi catalyst at high temperature and the second with the Cu catalyst at a lower temperature.

Keywords Water gas shift · Reactor design · Copper nickel catalysts · Hydrogen purification

---

✉ Eduardo Poggio-Fraccari
eduardoaristidespf@di.fcen.uba.ar

1 ITHES, UBA-CONICET, Pabellón de Industrias, Ciudad Universitaria,
1428 Ciudad Autónoma de Buenos Aires, Argentina

 Springer

Introduction

In the last years, non-traditional applications of hydrogen (such as electric power generation in fuel cells) have given rise to new research efforts to find active and stable catalysts for the water–gas shift (WGS) reaction. Proton-exchange membrane fuel cells (PEMFC) for mobile sources require that the inlet gas stream have a CO concentration lower than 20 ppm. Otherwise, the Pt-based anode is poisoned and the cell efficiency abruptly drops. Hence, if hydrogen is produced from a carbon containing raw material, a purification process must be carried out in order to reduce CO levels to cell requirements. So far, the technology most employed for H_2 purification consists of a WGS converter, reducing CO levels from typically 8–1%, and a latter step for the remaining CO elimination, until a concentration of 20 ppm is reached. According to Zalc and Löffler, the WGS reactor is expected to have the largest volume [1]. In chemical and petrochemical industrial applications, WGS is performed in two steps, the first which operates at high temperature (>400 °C) using Fe–Cr catalysts [2], and the second operating at lower temperatures (<250 °C) employing Cu–Zn-Al [3]. The renewed interest in the study of this reaction has resulted in several works published along the last 20 years, focused on finding alternative catalysts. Some authors proposed precious metal-based catalyst such as Pt [4, 5], Au [6–8], Pd, Rh, [9, 10] over different supports, as Al_2O_3, Fe_2O_3, TiO_2 or CeO_2, the latter being the most adequate support to enhance activity of catalysts. Besides, the performance of samples with less expensive transition metals, like Cu or Ni, supported on ceria, [11, 12], was investigated. More recently, it has been reported that the addition of lanthanide elements as La or Pr into ceria, enhances redox and textural properties [13, 14]. In a previous work, we explored the effect of Pr as a ceria promoter in high content Ni and/or Cu catalysts. We concluded that a small addition of ca. 5 wt% of Pr was the most suitable content to improve redox properties and WGS activities of Cu catalysts, and at the same time to mitigate the methanation reaction observed for Ni-based samples [15].

$$CO + H_2O \leftrightarrow CO_2 + H_2 \qquad (1)$$

$$CO + 3H_2 \leftrightarrow CH_4 + H_2O \qquad (2)$$

In the present work, an experimental study was conducted to understand the influence of active metal content analyzing a series of catalysts with 5, 10 and 20 nominal wt% of Cu and/or Ni. Samples with 10 wt.% of metal showed the best performance and were submitted to a kinetic study taking into account both reactions observed, i.e. WGS and methanation. According to the literature, power-law kinetics was previously proposed for the WGS reaction performed by catalysts based on transition metals as Pd, Pt, Rh, Ni, Cu, over ceria [10, 16, 17]. The authors fitted the experimental data to obtain the activation energy and reaction partial orders. These latter parameters were found to be close to unity. In the present work, we assumed simple reversible elementary kinetics for WGS reaction for all catalysts. To the best of our knowledge, no simultaneous fitting were previously reported for WGS and methanation in case of Ni-containing samples. For the latter

reaction, we also propose a reversible elementary kinetics with the stoichiometry of Eq. 2.

In this work, no CO_2 was used in the feed stream, since this is a first approach to the kinetic study. Further developments on the reaction mechanism will allow the consideration of both CO_2 and CH_4 gases. The kinetic expressions obtained were used to model single reactors or two-step reactor schemes using these catalysts with the aim of finding the configuration that minimize the total catalyst load, for the same feed conditions.

Materials and methods

Materials

Pr-promoted ceria support was obtained by the thermal treatment of a precursor synthesized by the urea thermal decomposition method [18]. This precursor was obtained by dissolving $Ce(NO_3)_3 \cdot 6H_2O$ (Fluka >99.0%) and $Pr(NO_3)_3 \cdot 6H_2O$ (Aldrich 99.9%) in distilled water in a molar ratio [Pr]/([Pr] + [Ce]) equal to 5 awt.% and total concentration of 0.1 M, and a urea concentration of 1 M at 90 °C for 24 h. After centrifuging and washing three times, a white solid was obtained. The calcination of the sample was conducted from room temperature to 450 °C with an air flow of 100 ml/min, a rate of 10 °C/min, maintaining this final temperature 450 °C for 5 h. Catalysts were prepared by incipient impregnation of the Pr-promoted ceria support with the corresponding metal salts: $Cu(NO_3)_2 \cdot 3H_2O$ (Sigma 98.0%) and/or $Ni(NO_3)_2 \cdot 6H_2O$ (Merck 99.0%). Salt concentrations were adjusted in order to obtain the desired metal loading for each catalysts, using a salt volume of 0.85 ml per gram of sample. After impregnation, catalysts were dried in a stove at 70 °C for 24 h and subsequently calcined following the same thermal treatment procedure as the support. The catalysts presented in this work were prepared with nominal metal contents of ca. 5, 10 and 20 wt%, and samples were named accordingly, i.e.: 5%Cu/CePr5 is a catalyst with 5 wt%. of pure Cu impregnated on Pr-promoted ceria. Besides, an additional bimetallic catalyst with 5 wt% Cu and 5 wt% Ni was prepared.

Experimental characterization and activity measurements

Three characterization techniques were used in this work. The surface area was obtained by sorptometry using an ASAP 2020 apparatus. The samples were characterized with X-ray diffraction (XRD) using the graphite-filtered Cu K_α radiation (λ = 1.5406 Å). Temperature programmed reduction (TPR) experiments were performed in a Micromeritics Auto Chem II 2920 analyzer equipped with a thermal conductivity detector. An H_2/Ar stream (4% H_2, 50 cm^3/min) was passed over 30 mg of the catalytic samples while the operating temperature was raised from room temperature to 1050 °C using a temperature ramp rate of 10 °C/min. Prior to TPR tests, the samples were treated at 450 °C for 1 h under a flow of air to clean the surface.

Activity tests were conducted in a stainless steel fixed-bed reactor using 120 mg of catalyst and a total inlet flow of 150 cm^3/min containing CO (8%), H$_2$O (24%), H$_2$ (45%) and N$_2$ as balance. The catalytic performance was evaluated at several temperatures in the range 250–450 °C. Before each analysis, solids were reduced for 30 min with a stream of H$_2$/N$_2$ (50% of H$_2$) at the highest reaction temperature employed (450 °C). At the reactor outlet, non-converted CO and gaseous products was analyzed by a Hewlett Packard HP 6890 gas chromatograph equipped with a TCD detector. Reported values of CO conversion correspond to steady state values, verified by the comparison of two successive chromatographic injections. Conditions used during activity test are listed in Table 1. The parameters used to evaluate the performance were the CO conversion, the selectivity to the WGS and the H$_2$ production ("ΔF_{H2}").

$$CO\,conversion = \frac{F_{CO}^{in} - F_{CO}^{out}}{F_{CO}^{in}} \cdot 100 \qquad (3)$$

$$WGS\,Selectivity = \frac{F_{CO2}^{out}}{F_{CO2}^{out} + F_{CH4}^{out}} \qquad (4)$$

$$\Delta F_{H2} = \frac{F_{H2}^{out} - F_{H2}^{in}}{F_{CO}^{in}} \qquad (5)$$

Kinetic parameter fitting

In order to fit the experimental data, reactions 1 and 2 were proposed for Ni containing catalysts (Ni and CuNi over CePr5), and only reaction 1 (i.e. WGS) was fitted in the case of Cu catalysts. The kinetic expressions employed to fit the data are:

$$r_1 = k_1 \left(p_{CO}p_{H_2O} - \frac{p_{CO_2}p_{H_2}}{K_{p1}} \right) \qquad (6)$$

Table 1 Activity test conditions

Condition	Value
Pressure (atm)	1.00
Volume flow (ml/min)	150.0
Catalyst mass (mg)	120
Gas hourly space velocity (h^{-1})	10,000
Catalyst mesh (μm)	44–88
p_{CO} (atm)	0.08
p_{H2O} (atm)	0.24
p_{H2} (atm)	0.45
p_{N2} (atm)	0.23

$$r_2 = k_2 \left(p_{CO} p_{H_2}^3 - \frac{p_{CH_4} p_{H_2O}}{K_{p2}} \right) \tag{7}$$

Here r_i is the reaction rate [mol/(min g)], k_i is the rate coefficient of reaction i (in consistent units), K_{pi} is the thermodynamic equilibrium constant of reaction i. Experimental conditions were such that no internal or external gradients of species compositions or temperature are present: in order to discard internal effects, different granulometry was employed until two consecutive sizes showed no difference in performance; for the case of external gradients, the gas flow was increased (changing the catalyst proportionally to maintain the contact time constant) until two different flows showed no appreciable variation in the performance of the fixed bed. This guaranteed the consideration of chemical control. Furthermore, plug flow conditions were fulfilled as well. Thus, with these considerations, we need to solve the set of mass balances for species j as shown in Eq. 8.

$$\frac{dF_j}{dm} = \sum_k^{N_R} \alpha_{jk} r_k = r_j \tag{8a}$$

$$F_j(m=0) = F_j^{in} \tag{8b}$$

The parameter fitting consisted in obtaining the values of the kinetic constants at each temperature. To this end, the error function is defined in Eq. 9:

$$G = \frac{1}{2} \sum_j \left[\ln \left(\frac{F_j^{calc}}{F_j^{dat}} \right) \right]^2 \tag{9}$$

Here F_j^{calc} is the outlet mole flow of j calculated by the simulation, F_j^{dat} represents the experimental data, α_{jk} are the stoichiometric factors of species j in reaction k. The aim is to find the value of the kinetic constants such that G attains the lowest possible value. This can be easily transformed into finding the zeros of Eqs. 10a and 10b for Ni and CuNi catalysts and Cu samples.

$$\boldsymbol{F} \triangleq \begin{bmatrix} \dfrac{\partial G}{\partial k_1} \\ \dfrac{\partial G}{\partial k_2} \end{bmatrix}, \boldsymbol{Y} \triangleq \begin{bmatrix} k_1 \\ k_2 \end{bmatrix} \tag{10a}$$

$$\boldsymbol{F} \triangleq \frac{\partial G}{\partial k_1}, \boldsymbol{Y} \triangleq k_1 \tag{10b}$$

These derivatives can be obtained numerically. With a goal function so defined, we solve the system by means of the Newton–Raphson method.

Once the values of the rate constants were obtained for each temperature, we finally fitted the pre-exponential factors and activation energies assuming an Arrhenius-type temperature dependence.

Simulation of reactors

The purpose of these simulations is to find the minimum catalyst load to attain a fixed (known) conversion. In this study, chemical control and plug flow conditions, as well as isothermal conditions, will be assumed. Even though these conditions most certainly will not hold for industrial scale reactors, it is useful to have an idea of around which temperature a non-isothermal reactor should operate at [19, 20]. Moreover, at lab scale, where the three previous conditions can be safely guaranteed, these calculations can lead to a better design of future experiences.

The following cases are considered:

I.   Single reactor with Cu catalysts
II. Single reactor with Ni catalysts
III. Single reactor with CuNi catalysts
IV. Two reactors, the first loaded with CuNi catalysts and the second with Cu catalysts.

With the above assumptions, the differential equations and initial conditions characterizing the mass balance for each species j are presented in Eq. 11. For cases I to III, the expression of the outlet flow is that of Eq. 12a, whereas for case IV, the expression is that that of Eq. 12b.

$$\frac{dF_j}{dm} = \sum_k^{N_R} \alpha_{jk} r_k = r_j \tag{11a}$$

$$F_j(m = 0) = F_j^{in} \tag{11b}$$

$$F_j^{out} = F_j^{in} + \int_0^M r_j dm \tag{12a}$$

$$F_j^{out,2} = F_j^{out,1} + \int_0^{M_2} r_j^2 dm = F_j^{in} + \int_0^{M_1} r_j^1 dm + \int_0^{M_2} r_j^2 dm \tag{12b}$$

Notice that m stands for the integration variable and M is the final value, i.e. the catalyst load. For a single reactor (cases I to III), we have to find the mass and the temperature such that $dM|_{F_{CO}^{out}} = 0$, whereas for two reactors (case IV), we have to find the temperature and the catalytic mass of both reactors such that $(dM_1 + dM_2)|_{F_{CO}^{out}} = 0$.

It is not easy to express the above condition of minimum since the dependence of the mass upon the other conditions is not straightforward. However, we can make use of the fact that the dependence of F_{CO}^{out} upon masses and temperatures is: by means of mass balances, we can explicitly calculate F_j^{out} from F_j^{in}, temperatures and catalyst loads. Thus, we invoke the implicit function theorem (see Supplementary Material for details) in order to yield the expressions sought. In this way, we finally obtain Eq. 13a for cases I to III, and Eq. 13b for case IV.

$$F \triangleq \begin{bmatrix} \dfrac{\partial F_{CO}^{out}}{\partial T} \bigg|_{M} \\ F_{CO}^{out} - \mathbb{C} \end{bmatrix} = 0, \ Y \triangleq \begin{bmatrix} T \\ M \end{bmatrix} \tag{13a}$$

$$F \triangleq \begin{bmatrix} \dfrac{\partial F_{CO}^{out}}{\partial T_1} \bigg|_{M_1, T_2, M_2} \\ \dfrac{\partial F_{CO}^{out}}{\partial M_1} \bigg|_{T_1, T_2, M_2} - \dfrac{\partial F_{CO}^{out}}{\partial M_2} \bigg|_{T_1, M_1, T_2} \\ \dfrac{\partial F_{CO}^{out}}{\partial T_2} \bigg|_{T_1, M_1, M_2} \\ F_{CO}^{out} - F_{CO}^{sought} \end{bmatrix} = 0, Y \triangleq \begin{bmatrix} T_1 \\ M_1 \\ T_2 \\ M_2 \end{bmatrix} \tag{13b}$$

The system is solved by means of the Newton–Raphson method. For further details about the development of the expressions and the numerical method, the reader is referred to the Supplementary Material.

Results and discussion

BET surface area and X-ray diffraction analysis

Samples were characterized by sorptometry, and BET values are reported in Table 2. As it can be seen, BET surface area decreases for metal-containing samples in comparison with the bare support. Values obtained for all catalysts were quite similar, irrespective of the active metal (Cu or Ni), except for the sample with the highest Ni content which is out the trend. The particle size was estimated from BET values assuming a spherical shape according to the equation reported by Colón et al. [21]. The decrease of the surface area in comparison with bare support indicates that particle size is larger for catalysts.

The X-ray pattern of the CePr5 support, reported in the supplementary material, shows typical fluorite reflections of CeO_2 (PDF No 42-1002) or PrO_2 (PDF 26-1349), which are very similar to each other. The same fluorite reflections were found in the patterns of all catalysts. This may suggest the presence of a solid solution for the support, where Pr was incorporated at fluorite lattice of ceria as it was already observed in the literature [13, 14]. Besides, in samples with 10 or 20 wt% metal loading, tenorite (CuO PDF No 45-0937) and bunsenite (NiO PDF No 47-1049) signals were also observed. This suggests that appreciable phase segregation occurs at these metal loadings. However, these peaks were not observed for contents up to 5 wt% in agreement with other authors [22, 23]. Hence, one can assume that active phases show an acceptable dispersion for both Cu and Ni catalysts.

Analyzing the crystal size of fluorite, estimated by the Scherrer equation and presented in Table 2, it was observed that the value was similar for catalysts and the bare support, indicating that no major changes were introduced in the crystalline structure during impregnation and calcination processes. However, the surface area

Table 2 BET and XRD results for bare support and catalysts

Sample	S_{BET} (m^2/g)	D_{BET} (nm)[a]	D_{XRD} (nm)[a]	$(D_{BET}/D_{XRD})^3$	CuO or NiO size (nm)
CePr5	100.2	8.3	8.0	1.1	–
5%Cu/CePr5	58.1	14.3	9.7	3.2	–
10%Cu/CePr5	58.0	14.4	9.9	3.1	23.7
20%Cu/CePr5	59.5	14.0	8.1	5.2	26.0
10%Cu–Ni/CePr5	57.3	14.5	9.8	3.2	–
5%Ni/CePr5	58.2	14.3	9.4	3.5	–
10%Ni/CePr5	57.8	14.4	9.8	3.2	18.0
20%Ni/CePr5	68.9	12.1	8.1	3.3	17.8

[a] Values corresponding to fluorite phase

of catalysts decreased. This feature can be explained comparing the volumes of particle and crystal by using their sizes (D_{BET} by BET results, D_{XRD} estimated by the Scherrer formula), i.e. $(D_{BET}/D_{XRD})^3$ reported in Table 2. The results show that crystal agglomeration is responsible for the lower surface area found for the catalysts in comparison with bare support.

CuO and NiO reflections in XRD patterns were also studied, and the results presented in Table 2. The CuO crystal size was always higher than that of NiO, suggesting that the former is more sensitive to sintering during the calcination step, than the latter. This observation can be explained by the Tamman–Huetig criterion, which states that the sintering temperature of a material is proportional to its melting point, and CuO has a lower melting temperature than NiO, 1326 and 1950 °C, respectively [24]. As for the CuNi bimetallic sample, according to previous analyses, a similar behavior of those monometallic with 10 wt% is observed, where no surface segregation was found, suggesting that the active phase is highly dispersed over sample surface.

Temperature programmed reduction

Catalysts were submitted to a reducibility analysis and their reduction profiles at 100–400 °C range are shown in Figs. 1 and 2 for Cu and Ni solids, respectively, and complete profiles are shown at supplementary material. The bare support shows two reduction regions, marked as α (low temperature region close to 470 °C) and β (high temperature region, peak ca. 830 °C) [18]. The former is related to the reduction of superficial ions, and the latter to bulk reduction of Ce^{4+} and Pr^{4+}. The α region is absent in all Cu and Ni samples, but β regions are still present, although a slight displacement was observed when metals were added to CePr5.

Cu catalysts show profiles completely different from those of the bare support, with several peaks at 100–250 °C, a temperature range lower than the α region (Fig. 1). When compared to bulk CuO, events also take place at a lower reduction temperature (approximately 260 °C). Therefore, it is concluded that CePr5
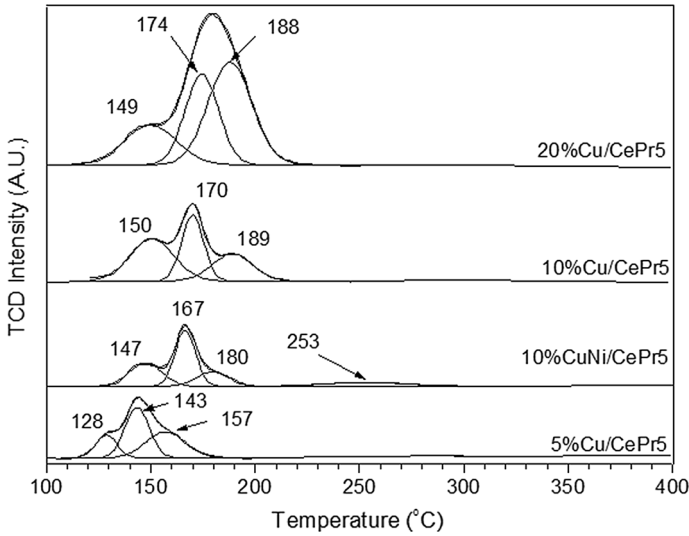
Fig. 1 Deconvolution of TPR profiles of copper samples, 60 mg of mass, 50 ml/min of Ar (2% of H_2), and temperature ramp 10 °C/min
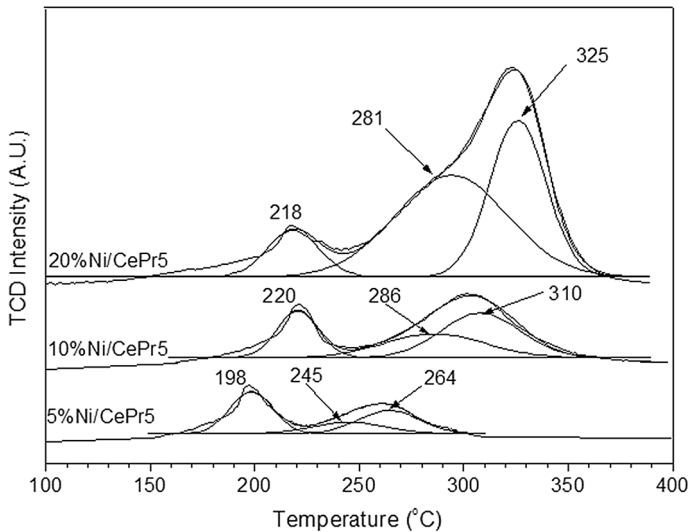

Fig. 2 Deconvolution of TPR profiles of nickel samples, 60 mg of mass, 50 ml/min of Ar (2% of H_2), and temperature ramp 10 °C/min

significantly promotes copper reducibility for all metal loadings analyzed in this work. Table 3 displays H_2 consumption for all samples showing that these values are higher than the stoichiometric consumption required to reduce all Cu^{2+} ions to Cu^0. This indicates that some Ce^{4+} and Pr^{4+} ions were reduced together with copper ions during low temperature events. It can be concluded that CePr5 and Cu exhibit a

synergic reduction effect for all metal loadings examined in this work, in agreement with observations reported in the literature for copper over ceria catalysts [11, 25].

Bimetallic catalysts show reduction events in the same temperature region as Cu-based solids, indicating similar reducibility. However, an additional peak centered at 246 °C appears and H_2 consumption is quite similar to the theoretical value required to reduce all cations (Cu^{2+} and Ni^{2+}) in the active phase. This suggests that Cu^{2+} and Ni^{2+} species are interacting and, consequently, a deconvolution analysis of the profiles was performed. Luo et al. prepared ceria samples with Cu contents between 0.5 and 15 wt% and found a bimodal reduction profile in the range 120–200 °C [26]. For the second peak, these authors observed a shift towards higher temperatures with metal content and concluded that this peak corresponded to agglomerated particles. Other authors also found at least two peaks in the range 120–250 °C for copper over ceria solids, arguing that events at low temperature are related to the reduction of copper species interacting with ceria support, and high temperature events to bulk CuO reduction [27]. Besides, Caputo et al. reported several reduction peaks for their copper-ceria system, which were assigned to highly dispersed copper at 130 °C, copper incorporated to ceria lattice at 150 °C, and segregated Cu^{2+} at 200 °C [15]. The discussion on this topic was previously reported for samples of copper over pure ceria, and not for Cu over Pr-promoted ceria supports. However, considering that events for Cu over ceria occurred in the same reduction temperature range as those observed for Cu over CePr5 support, the same peak assignment might be suggested for the catalysts presented in this work. Since 5%Cu/CePr5 has the most reducible species (see Fig. 1), this implies that events correspond to highly dispersed Cu^{2+} particles more interacting with support ions, due to the fact that the H_2 uptake is almost twice the theoretical value (see Table 3). The increase of copper loading to 10 wt.% modifies the reduction profile shifting events towards high temperatures, but a further addition up to 20 wt% did not show significant changes; in fact, not only are peak positions similar, but also peak widths, meaning that same species are present in both samples. This suggests that reducibility is not enhanced by higher copper loadings. Moreover, for samples with 10 and 20 wt%, CuO phase reflections were found in XRD patterns, indicating that crystal agglomeration occurred, and high temperature events correspond to the

Table 3 H_2 uptake during TPR experiments and theoretical consumption needed to reduce $Ce^{4+} \rightarrow Ce^{3+}$, $Cu^{2+} \rightarrow Cu^0$ and $Ni^{2+} \rightarrow Ni^0$

Samples	H_2 uptake (mmol H_2/g_{cat})	Theoretical H_2 uptake (mmol H_2/g_{cat})
CePr5	0.4	2.9[a]
5%Cu/CePr5	1.7	0.6
10%Cu/CePr5	1.5	1.2
20%Cu/CePr5	2.8	2.4
10%CuNi/CePr5	1.1	1.3
5%Ni/CePr5	0.8	0.7
10%Ni/CePr5	0.9	1.3
20%Ni/CePr5	2.2	2.6

[a] Uptake needed to reduce Ce^{4+} a Ce^{3+}

reduction of segregated Cu^{2+} species, with low interaction with Ce^{4+} and Pr^{4+} ions. It is worth mentioning that the H_2 uptake is similar to the theoretical value, bearing out a weaker interaction of the active phase with the support. The bimetallic sample shows a similar profile compared to high copper-content monometallic samples in 130–180 °C range. A small peak close to 250 °C was found, which could be related to reduction of Ni particles. According to the H_2 consumption, some support ions are reduced, which implies that Cu^{2+} and Ni^{2+} particles are interacting with Ce^{4+} and Pr^{4+} in all reduction events.

TPR experiments were also carried out for nickel containing catalysts (Fig. 2). More complex profiles were found in comparison with previous reports, with peaks centered at higher temperatures in comparison to copper, indicating the lower reducibility of Ni samples. A small peak close to 200 °C in 5% Ni/CePr5 shifts towards higher temperatures in samples with 10 and 20 wt% of Ni, and its intensity decreases. The region that initiates at 230 °C also shifts to higher temperatures and its area markedly increases with Ni addition. In all cases, peaks were found at temperatures lower than those of NiO (350–550 °C) and CePr5 (α and β region). This feature suggests that the support favors metal dispersion and, therefore, sample reducibility. A qualitative analysis of profiles of nickel over Pr-doped ceria was not found in literature. However, some authors reported a peak assignment for Ni/CeO_2. These authors observed three events in the 200–400 °C temperature range: aggregated NiO species, highly dispersed NiO with strong interaction with CeO_2, and Ni incorporated in ceria lattice [28]. Chary et al. prepared Ni Ceria catalysts by impregnation and co-precipitation [29]. These authors reported similar profiles for both samples, but reduction events shift to higher temperatures for the co-precipitated one, suggesting that a strong interaction between Ni and Ce is responsible for this shift. Nevertheless, other authors disagree with the assignment of the high temperature event, claiming that it is related to the reduction of NiO clusters over the ceria surface [30]. For the samples studied in the present work, the reduction profiles present at least three events, in a similar temperature range as in the aforementioned Ni over unpromoted-ceria (Fig. 2). The 5%Ni/CePr5 sample show peaks at lower temperatures compared to the remaining samples: the first peak, which is probably associated to free Ni^{2+} species, changes its position from 198 °C in the 5 Ni wt% catalyst to temperatures close to 220 °C in the other two Ni catalysts. According to XRD patterns, high metal content samples show bunsenite reflections, indicating the presence of segregated bulk NiO particles, which are less reducible and might be related to reduction events at temperatures higher than 240 °C in TPR profiles. It should be noted that a simultaneous change in the oxidation state of Ni^{2+} and support ions, Ce^{4+} and Pr^{4+} could not be discarded.

Water gas shift activity

Fig. 3 shows the CO conversion attained at the outlet of the experimental fixed-bed reactor using Cu catalysts at reaction conditions previously reported in "Experimental characterization and activity measurements" section. CO conversion increases with reaction temperature and copper loading of the samples (reaching 50% at 450 °C for 20% Cu/CePr5 sample). The catalytic performance significantly

increases for 10 wt% metal loading, in comparison with the 5 wt% sample. However, a small difference in CO conversion was found with a further increase, from 10 to 20 wt%. Qi and Flitzany-Stephanopoulos, reported this same trend for their copper-ceria-lanthana co-precipitated catalysts. The Cu content was modified in a wide concentration range among 5 and 15 wt%, and conversion values were quite similar for 5, 10 and 15 wt% loadings [16].

On the other hand, the catalytic performance of nickel-containing samples is presented in Fig. 5, and it can be seen that CO conversions area higher than copper samples. In fact, CO conversion values are close to 100% in the temperature range 375–450 °C. The monometallic sample with 5 wt% of metal content shows the lowest activity, while no appreciable differences are found for solids with 10 or 20 Ni wt% of Ni.

For these samples, CH_4 was detected at the reactor outlet stream, suggesting that sites not only are active to the WGS reaction, but also to methanation. It was widely reported that nickel over ceria is an effective catalyst for methanation reactions [31–33]. In fact, in a previous work, we studied the effect of Pr as a promoter to enhance WGS selectivity by minimizing the extent of the methanation reaction. We concluded that the optimum Pr content, in the mixed Ce–Pr oxides used as support of nickel catalysts, was close to 5 wt% [18]. Since the catalysts studied in the present work show activity for CH_4 production, it is necessary to quantify the undesired methanation occurrence making use of WGS selectivity defined in Eq. 2. The corresponding selectivity values are reported in Fig. 5. As can be seen, the tendency to form CH_4 increases with the reaction temperature and with Ni loading in samples, although selectivity values are almost constant for 10 and 20 samples above 350 °C. In summary, Figs. 5 and 6 suggest that the catalytic behavior of
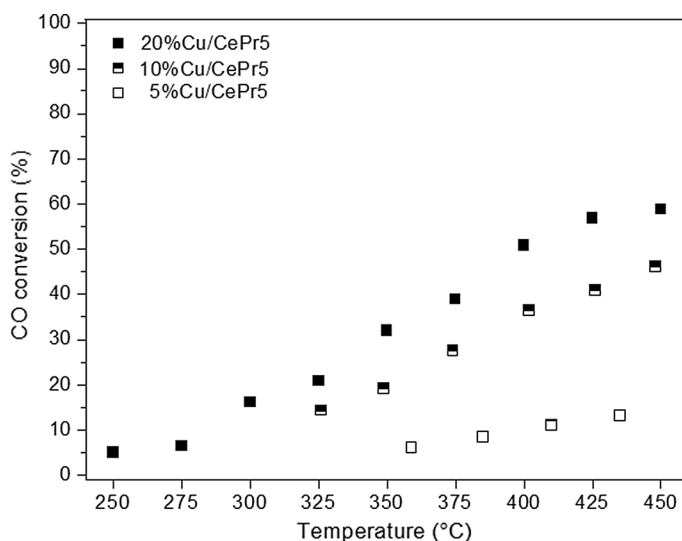

Fig. 3 CO conversion vs. temperature for Cu-containing catalysts, mass: 120 mg, 150 ml/min of total flow (8% CO, 24% H2O, 45 H_2, N_2 as balance)

monometallic Ni catalysts becomes independent of active me wt%tal loading for contents higher than 10 wt%.

Recently other authors studied bimetallic CuNi catalysts over redox supports for the WGS reaction. Lin et al. reported a large selectivity (>95%) for their CuNi high metal content samples supported over ceria-lanthana tested in the 150–500 °C temperature range with a feed containing 10% of CO, 20% H_2O and He as balance [34]. Shinde and Madras impregnated Cu and Ni over ceria and tested these catalysts in a feed stream of 2 vol.% of CO, 55 vol.% of H_2O and N_2 as balance at 100–450 °C [35]. None of these authors found considerable amounts of CH_4 or other hydrocarbons at the reactor outlet, but it should be remarked that these works have used synthetic feed streams that only contained CO and H_2O, in contrast with this work, where H_2 is also added at the reactor inlet. Metal content screening shows that 10 wt% samples have an acceptable activity-selectivity ratio. With this information, a bimetallic sample was prepared with the same total content (5 wt% Cu and 5 wt% Ni), and tested.

As it can be seen in Fig. 4, by the comparison at the same total metal content, the CuNi catalyst shows an activity higher than the monometallic Cu sample (see Fig. 3), but lower than that of Ni. On the other hand, the selectivity of the bimetallic solid was superior to those of all Ni catalysts in the whole temperature range (Fig. 5). Moreover, the CH_4 concentration at the reactor outlet for the CuNi catalyst was negligible. Similar features were already observed in our previous work for bimetallic samples with different CuNi ratios [15]. Evidence was found in the literature to support the formation of a CuNi alloy under reducing atmospheres, as it is the case of WGS conditions, which might also be responsible of the high
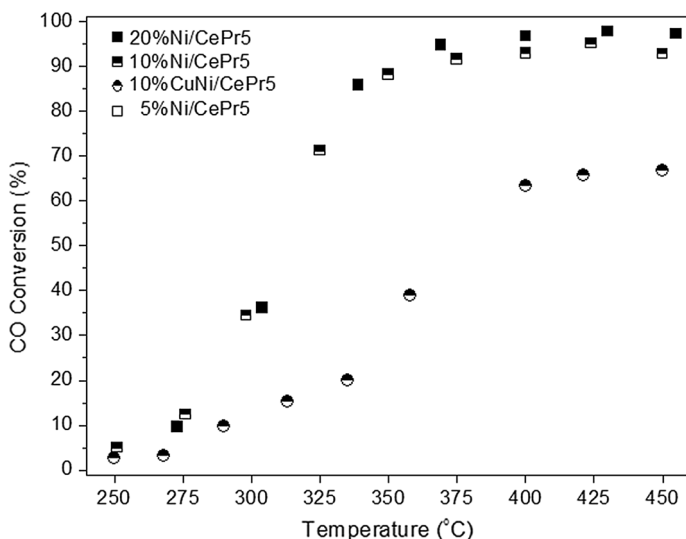

Fig. 4 CO conversion vs. temperature for Ni-containing catalysts, mass: 120 mg, 150 ml/min of total flow (8% CO, 24% H_2O, 45 H_2, N_2 as balance)
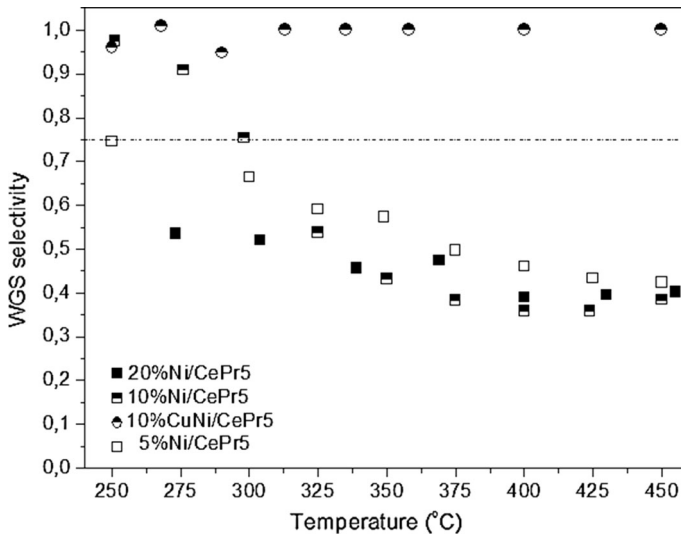
Fig. 5 WGS selectivity of Ni-containing catalysts measured during activity conditions

selectivity values [34]. However, this alloy was not be detected in our high metal-dispersed bimetallic sample in the XRD patterns.

In summary, the monometallic samples with 10 wt% have shown an acceptable catalytic performance, with Cu, CuNi and Ni active metals. Hence, these three samples were chosen to perform a kinetic study in order to simulate the single or two-stage WGS reactors.

Kinetic fitting

The feed conditions, pressure and catalyst mass used for numerical fitting are listed in Table 1, "Experimental characterization and activity measurements" section. The specific rate constants for reactions 1 and 2, WGS and CO methanation were fitted for several temperatures, as it was mentioned in "Kinetic parameter fitting" section. For further information about the goodness of the fit, see the supplementary material.

By using an Arrhenius-type temperature dependence, activation energies E_{act} and pre-exponential factors k_o were obtained and reported in Table 4 along with R^2 correlation factors.

The E_{act} found for Cu catalysts is lower than those for both Ni-containing solids, suggesting that the former are more active at low temperature. This trend is in agreement with the literature for similar catalyst systems, where Cu/CeO_2 catalysts presented lower activation energy than Ni/CeO_2 [16].

For Cu-containing solids, the activation energy obtained for the WGS reaction is similar to those reported by other authors, i.e. in the range 40–55 kJ/mol for Cu over ceria samples with similar metal loading and tested in temperatures ranging 250–400 °C [36–38]. Conversely, the comparison for Ni samples is more difficult

Table 4 Results of kinetic fitting for WGS and CO methanation

Sample	WGS reaction			CO methanation		
	ln (ko)[a]	E_{act} (kJ/mol)	R^2	ln (ko)[b]	E_{act} (kJ/mol)	R^2
10%Cu/CePr5	1.23	42.0	0.99	–	–	–
10%Ni/CePr5	6.98	70.0	0.96	15.66	104.5	0.98
10%CuNi/CePr5	9.16	82.6	0.99	17.13	142.5	0.99

[a] Ko constant for WGS in mol/(g s atm^2)

[b] Ko constant for CO methanation in mol/(g s atm^4)

since data in literature is scarce. The value obtained in the present work was close to 70 kJ/mol, similar to 85 kJ/mol reported by Wheeler et al. for their Ni/CeO_2 sample [17]. As it was mentioned in the previous section, only recently have bimetallic samples for WGS gained attention, and thus no E_{act} for WGS were found in literature.

Reactor simulation

In this section, we show the performance of the system when the minimum catalyst load required to attain a given conversion is sought. It is worth noting that we are looking for optima restricted to the temperature range 250 °C ≤ T ≤ 450 °C. Thus, in some cases, we shall find unbounded minima (like in Cu-catalysts), and in others, we shall find that the minimum is at the boundary in the temperature range. For the sake of comparison, a dimensionless contact time defined as the ratio between simulation and experiments, $\theta_{sim}/\theta_{exp}$ (which is numerically equal to the ratio of the mass obtained by simulation and that used in experiments, since flows are the same) is hereafter used to report results.

Simulation of a single reactor

When performing the unrestricted optimization, it was observed that for the case of CuNi and Ni catalysts, the temperatures obtained for the whole range of conversions analyzed were beyond the calcination temperature (450 °C). The same happened for the Cu catalyst for low conversions. Thus, it was decided to set the temperature to the maximum allowed, i.e. 450 °C, whenever the optimization yielded a higher value. See supplementary material for further details. Fig. 6 summarizes the results given the temperature restriction.

From the point of view of minimizing the mass, it is apparent that a Ni-based catalyst should be used to attain any final conversion within the range surveyed. However, Fig. 7 shows that H_2 production, as defined in Eq. 3, is negative for this case. An intermediate behavior is found for CuNi-based catalysts, in which for x < 83% the net H_2 production is positive. Finally, Cu catalysts are the best choice for H_2 yield, but the worst in terms of mass required.
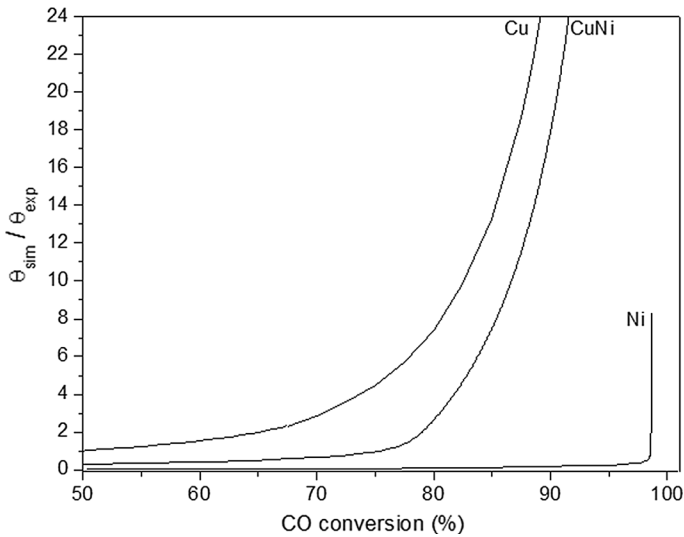
Fig. 6 Dimensionless contact time versus conversion sought for single-reactor simulation obtained for 10 wt% catalysts with temperature restriction at 450 °C CuNi and Ni samples

As for the catalyst load, for the case of CuNi, notice that there is a strong change of the slope in the curve for x ≈ 78% (Fig. 6), which must be related to a sudden decrease of the reaction rate. In order to explain this behavior, we show the extent of both reactions considered in Fig. 8, plotted as a dimensionless value related to the CO inlet reactor molar flow. By analyzing the slope of these curves, which are proportional to the reaction rates, it can be seen that at low catalyst loads, reaction rate 1 (WGS) is dominant over reaction 2 (methanation). However, it can be seen that from a dimensionless contact time equal to 1.33, the WGS reaction becomes zero (derivative equal to 0), and then this derivative turns negative, which means that it reverses its sense. On the other hand, the methanation reaction is always positive and increases with contact time.

The fact that reaction 1 markedly slows (and even reverses) whereas reaction 2 does not can be explained in terms of the vicinity of each reaction to their corresponding states of equilibrium. It is worth mentioning that the WGS reaction is allowed to surpass its equilibrium condition and change its sense because there is another reaction occurring [39–41]. The supplementary material provides more information about this issue. After the maximum in the extent of the WGS reaction, the slopes (i.e. the reaction rates) are of similar magnitude, but with opposite signs. This means in turn that the net rate of CO reaction is now the difference (and not the sum) of the contributions of both reactions and as a consequence, more room is needed for the net CO consumption to proceed. Therefore, from this point, mass grows faster for higher conversions (Fig. 6). It is for the same reason that H_2 yield markedly decreases from this value on (Fig. 7).
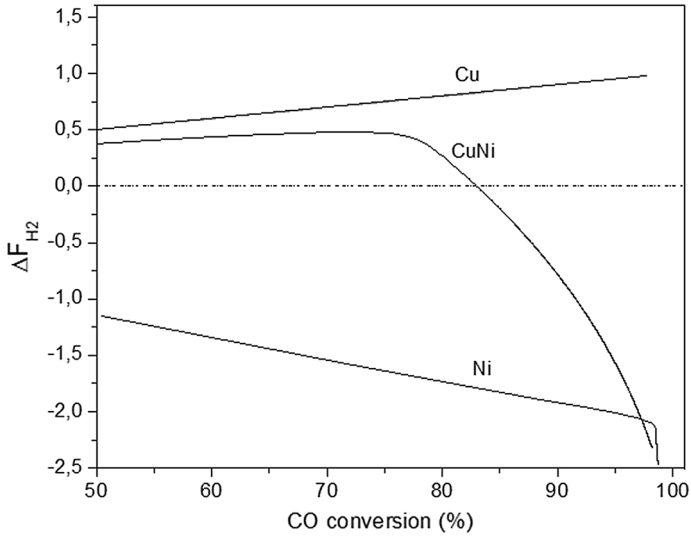
Fig. 7 H_2 yield versus conversion sought for single-reactor simulation obtained for 10 wt% catalysts with temperature restriction at 450 °C CuNi and Ni samples
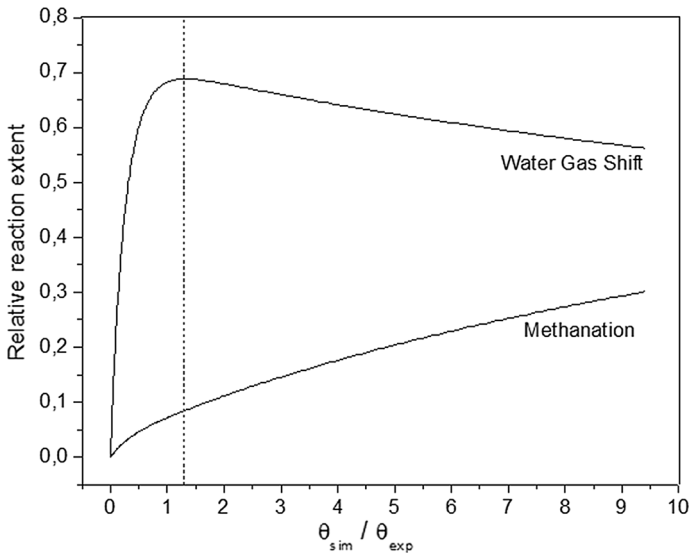

Fig. 8 Reaction extent relative to CO molar feed for reactions 1 (WGS) and 2 (methanation) versus dimensionless contact time, for CuNi sample at 450 °C and CO conversion equal to 78%

It is for this reason that we acknowledge a limit in the relationship conversion/selectivity/catalyst load for a single reactor regardless of the catalyst employed. With the aim of obtaining high conversions with minimum catalyst load and maintaining a positive H_2 yield (i.e. high selectivity), the use of more than one

reactor arises as an alternative, which enables to exploit the advantages of Cu catalysts for H_2 yield and those of CuNi or Ni catalysts in lower mass required.

Simulation of two reactors

Results for a two-reactor scheme are shown only for the case of CuNi + Cu array since for Ni + Cu, the mass required was always lower for a Ni single reactor. It should be remembered that the study was based on optimizing the total mass irrespective of selectivity values obtained: the latter is a consequence of the mass minimization, recall Fig. 7.

For the case of CuNi + Cu array, the optimization showed that it is convenient to operate both reactors at a higher temperature compared to their single-reactor counterparts. However, this is not possible since, for the CuNi reactor, we would be operating at T > 450 °C. Thus, it was decided to set the CuNi reactor at the highest possible temperature, as it was already done for the single-reactor case, i.e. T = 450 °C.

Simulation results with temperature restriction are reported in Figs. 9 and 10. From the point of view of minimizing the total mass, it can be seen that until a conversion of ca. 78%, a single CuNi reactor operated at 450 °C is the best choice. For higher conversions, a scheme of two reactors is better than the single CuNi reactor at 450 °C. The need of a second reactor occurs at the conversion at which the WGS get very close to equilibrium, i.e. close to 78% (see supplementary material for more details). The second reactor operating at a lower temperature than the first drives the system out of equilibrium. In addition, the two-reactor scheme proposed enhances the H_2 yield when compared to the single one with CuNi solid and extends the range of positive H_2 production from x = 83% to x = 91%.
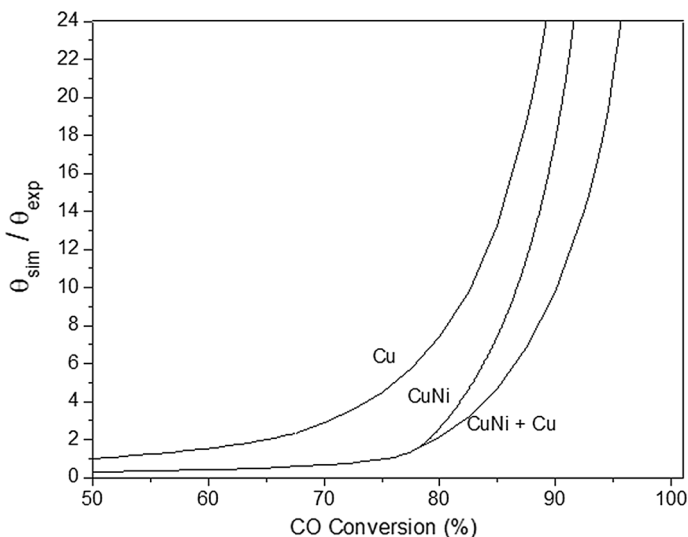

Fig. 9 Dimensionless contact time versus conversion sought for single- and two-reactor schemes (with 450 °C for the reactor operating with CuNi sample)
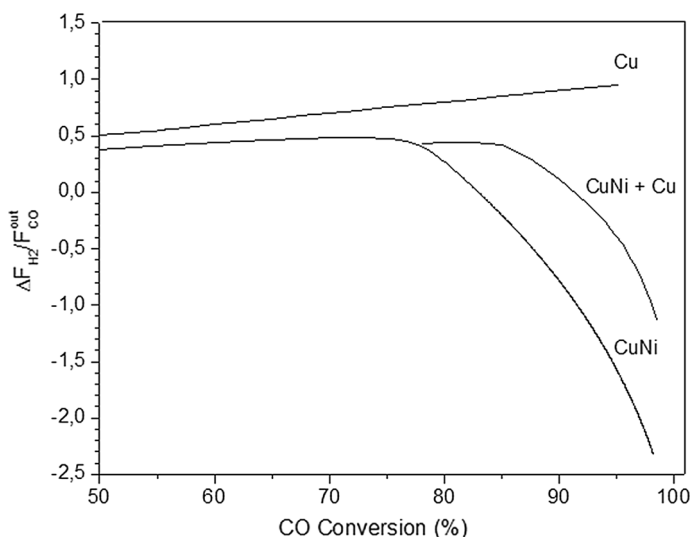
Fig. 10 H_2 yield vs. dimensionless contact time for single- and two-reactor schemes (with 450 °C restriction for the reactor operating with CuNi sample)

Conclusions

Several Cu and/or Ni catalysts supported on Pr-doped ceria were characterized and tested in WGS reaction during the present work. XRD patterns of the samples showed appreciable phase segregation (CuO or NiO) for 10 and 20 wt% samples. The reducibility of the samples significantly changed when metal content was increased from 5 to 10 wt%, but no major differences in reduction profiles were observed among 10 and 20 wt% samples, irrespectively of the metal, Cu or Ni. A similar behavior was found in the catalytic performance of the samples. The CO conversion significantly increased for samples with a middle content (10 wt%) in comparison with the lowest metal loading (5 wt%). However, CO conversion did not increase for a higher loading (20 wt%), suggesting that phase segregation, reducibility and activity are related. A bimetallic CuNi catalyst (total metal content 10 wt%) was also prepared and evaluated, and it showed better activity than the monometallic 10% Cu/CePr5 sample, and higher selectivity than the 10% Ni/CePr5. The analysis of the reduction profile revealed that metallic copper enhanced reducibility of Ni^{2+} species. According to the XRD patterns, NiO phase segregation was not observed in the bimetallic catalyst, in contrast to the segregation found for the corresponding monometallic Ni sample, which could explain the higher selectivity of the former.

Kinetic studies and reactor modelling were performed for three catalysts with 10 wt% metal loading (Cu, Ni and bimetallic CuNi). By fitting the experimentally observed CO conversion, activation energies were obtained simultaneously for WGS and CO methanation reactions following an approach not reported in the literature despite the widely known occurrence of CO methanation over Ni

catalysts. Cu catalysts showed lower activation energy for the WGS reaction than the Ni sample, in agreement with the trend reported in the literature. By modelling a single reactor, it was observed that the catalytic mass required to attain the conversion sought depends on the sample considered, following the trend Cu > CuNi > Ni. However, appreciable H_2 loss was also found in the case of a reactor operating with Ni sample. An analysis performed for the CuNi sample demonstrated that WGS rate becomes very small for conversions higher than 78%, value from which CO methanation is the only reaction that virtually takes place. This result implies that appreciable methanation will inevitably occur when high conversions are required. Therefore, a two-reactor scheme was proposed as an alternative to achieve high CO conversions and retain acceptable selectivity to WGS. The most promissory combination of catalysts found was the bimetallic CuNi sample for the first reactor and the monometallic Cu catalyst for the second, the former operating temperatures higher than the latter. Compared to the CuNi-based catalyst single-reactor, the two-reactor scheme was better in terms of both mass and H_2 yield. Taking $\Delta F_{H_2} = 0$, i.e. no net H_2 production, as a limiting value, the former should be used up to a conversion of ca. 83%, whereas for the latter, the use can be extended up to a conversion of ca. 91%. Compared to the Cu-based catalyst single-reactor case, the two-reactor scheme employs less mass for the same service, but produces less H_2 because of the presence of Ni (i.e. the occurrence of methanation). Overall, it is concluded that the most promissory combination of catalysts found the two-reactor scheme, the first operating at high temperature with the bimetallic CuNi catalyst, and the second at lower temperatures with the monometallic Cu catalyst.

The fact that the WGS reaction attains equilibrium while the methanation does not suggest that either new formulations of catalysts should be found that minimize the methanation reaction or reactors should operate at different temperatures in order to avoid this equilibrium approach.

References

1. Zalc M, Löffler D (2002) Fuel processing for PEM fuel cells: transport and kinetic issues of system design. J Power Sour 111:58–64
2. Amadeo N, Laborde M (1995) Hydrogen production from the low-temperature water–gas shift reaction: kinetics, and simulation of the industrial reactor. Int J Hydrog Energy 20:949–956
3. Ratnasamy C, Wagner J (2009) Water gas shift catalysis. Catal Rev 51:325–440
4. Panagiotopoulou P, Papavasiliou B, Avgouropoulos J, Ionnides G, Kondarides T (2007) Water gas shift activities of doped Pt-CeO$_2$ catalysts. Chem Eng J 134:16–22
5. Tiwari R, Sarkara B, Tiwari R, Pendem C, Sasaki T, Saran S, Bal R (2014) Pt nanoparticles with tuneable size supported on nanocrystallineceria for the low temperature water–gas-shift (WGS) reaction. J Mol Catal 395:117–123
6. Reina T, Ivanova S, Centeno M, Odriozola J (2015) Boosting the activity of a Au/CeO$_2$/Al$_2$O$_3$catalyst for the WGS reaction. Catal Today 253:149–154
7. El-Moemen A, Karpenko A, Denkwitz Y, Behm R (2009) Activity, stability and deactivation behavior of Au/CeO$_2$ catalysts in the water gas shift reaction at increased reaction temperature (300 °C). J Power Sourc 190:64–75

8. Mendes D, Garcia H, Silva V, Mendes A, Madeira M (2009) Comparison of nanosized gold-based and copper-based catalysts for the low-temperature water–gas shift reaction. Ind Chem Res. 48:430–439

9. Jacobs G, Chenu E, Patterson P, Williams L, Sparks D, Thomas G, Davis B (2004) Water–gas shift: comparative screening of metal promoters for metal/ceria systems and role of the metal. Appl Catal A Gen 258:203–214

10. Bunluesin T, Gorte R, Graham G (1998) Studies of the water-gas-shift reaction on ceria-supported Pt, Pd, and Rh: implications for oxygen-storage properties. Appl Catal B Environ 15:107–114

11. Qi X, Flytzani-Stephanopoulos M (2004) Activity and stability of Cu-CeO$_2$ catalysts in high-temperature water–gas shift for fuel-cell applications. Ind Eng Chem Res 43:3055–3062

12. Gunawardana P, Lee H, Kim D (2009) Performance of copper–ceria catalysts for water gas shift reaction in medium temperature range. Int J Hydrog Energy 34:1336–1341

13. Reddy B, Thrimurthulu G, Katta L, Yamada Y, Park S (2009) Structural characteristics and catalytic activity of nanocrystalline ceria-praseodymia solid solutions. J Phys Chem C 113:15882–15890

14. Borchert H, Frolova Y, Kaichev V, Prosvirin I, Sadykov V (2005) Electronic and chemical properties of nanostructured cerium dioxide doped with praseodymium. J Phys Chem C 109:5728–5738

15. Poggio-Fraccari E, Mariño F, Laborde M, Baronetti G (2013) Copper and nickel catalysts supported on praseodymium-doped ceria (PDC) for the water–gas shift reaction. Appl Catal A Gen 460:15–20

16. Li Y, Qi F, Flytzani-Stephanopoulos M (2002) Low-temperature water-gas shift reaction over Cu- and Ni-loaded cerium oxide catalysts. Appl Catal B Environ 27:179–191

17. Wheeler C, Jhalani A, Klein E, Tummala S, Schmidt L (2004) The water–gas-shift reaction at short contact times. J Catal 223:191–199

18. Poggio-Fraccari E, Irigoyen B, Baronetti G, Mariño F (2014) Ce-Pr mixed oxides as active supports for water–gas shift reaction: experimental and density functional theory characterization. Appl Catal A Gen 485:123–132

19. Giunta P, Moreno M, Mariño F, Amadeo N, Laborde M (2012) COPROX fixed bed reactor temperature control schemes. Chem Eng J 35:1055–1063

20. Jeifetz L, Giunta P, Mariño F, Amadeo N, Laborde M (2014) Simulation of CO preferential oxidation (COPrOx) monolithic reactors. Int J Chem React Eng 12:1–12

21. Colón G, Pijolat M, Valdivieso F, Vidal H, Kaspar J, Finocchio E (1998) Surface and structural characterization of Ce$_x$Zr$_{1-x}$O$_2$ CEZIRENCAT mixed oxides as potential three-way catalyst promoters. J Chem Soc Faraday Trans 94:3717–3726

22. Jobbágy M, Mariño F, Schönbrod B, Baronetti G, Laborde M (2006) Synthesis of copper-promoted CeO$_2$ catalysts. Chem Mater 18:1945–1950

23. Rico-Pérez V, Aneggi E, Bueno-López A, Trovarelli A (2016) Synergic effect of Cu/Ce$_{0.5}$Pr$_{0.5}$O$_{2-x}$ and Ce$_{0.5}$Pr$_{0.5}$O$_{2-x}$ in soot combustion. Appl Catal B Environ. 197:95–104

24. Moreira M, Ribeiro A, Cunha A, Rodrigues A, Zabilsky M, Djinovic P, Pintar A (2016) Copper based materials for water-gas shift equilibrium displacement. Appl Catal B Environ 189:199–209

25. Caputo T, Lisi L, Pirone R, Russo G (2008) On the role of redox properties of CuO/CeO$_2$ catalysts in the preferential oxidation of CO in H$_2$-rich gases. Appl Catal A Gen 328:42–53

26. Luo M, Zhong Y, Yuan X, Zheng X (1997) TPR and TPD studies of CuO/CeO$_2$ catalysts for low temperature CO oxidation. Appl Catal A Gen 162:121–131

27. Rao G, Sahu H, Mishra B (2003) Surface and catalytic properties of Cu–Ce–O composite oxides prepared by combustion method. Coll Surf A 220:261–269

28. Du X, Zhang D, Shi L, Gao R, Zhang J (2004) Morphology dependence of catalytic properties of Ni/CeO$_2$ nanostructures for carbon dioxide reforming of methane. J Phys Chem C 116:10009–10016

29. Chary K, Rao P, Vishwanathan V (2006) Synthesis and high performance of ceria supported nickel catalysts for hydrodechlorination reaction. Catal Commun 7:974–978

30. Liu W, Flitzany-Stephanopoulos M (1995) Total oxidation of carbon monoxide and methane over transition metal-fluorite oxide composite catalyst. J Catal 153:317–332

31. Fatsikostas A, Verykios X (2004) Reaction network of steam reforming of ethanol over Ni-based catalysts. J Catal 225:439–452

32. Huang T, Yu T, Jhao S (2006) Weighting variation of water–gas shift in steam reforming of methane over supported Ni and Ni–Cu catalysts. Ind Eng Chem Res 45:150–156

33. Zyryanova M, Snytnikov P, Amosov Y, Kuzmin V, Kirillov V, Sobyanin V (2001) Design, scale-out, and operation of a preferential CO methanation reactor with a nickel ceria catalyst. Chem Eng J 176:106–113

34. Lin J, Biswas P, Guliants V, Misture S (2010) Hydrogen production by water–gas shift reaction over bimetallic Cu–Ni catalysts supported on La-doped mesoporous ceria. Appl Catal A Gen 387:87–94
35. Shinde V, Madras G (2002) Water gas shift reaction over multi-component ceria catalysts. Appl Catal B Environ 123:367–378
36. Koryabkina N, Phatak A, Ruettinger W, Farrauto R, Ribeiro F (2003) Determination of kinetic parameters for the water–gas shift reaction on copper catalysts under realistic conditions for fuel cell applications. J Catal 217:233–239
37. Zerva C, Philippopoulos C (2006) Ceria catalysts for water gas shift reaction: influence of preparation method on their activity. Appl Catal B Environ 67:105–112
38. Si R, Raitano J, Yia N, Zhang L, Chan S, Flytzani-Stephanopoulos M (2012) Structure sensitivity of the low-temperature water–gas shift reaction on Cu–CeO$_2$ catalysts. Catal Today 180:68–80
39. Strogatz S (1994) Nonlinear dynamics and chaos, 1st edn. Addison-Wesley Reading, Boston
40. Prigogine I (1961) Introduction to thermodynamics of irreversible processes, 2nd edn. Wiley, New York
41. de Groot S, Mazur P (1985) Non-equilibrium thermodynamics, 2nd edn. Dover Publications Inc., New York